Journal of Catalysis 276 (2010) 6–15

Contents lists available at ScienceDirect

Journal of Catalysis

journal homepage: www.elsevier.com/locate/jcat

Role and advantages of H_2S in catalytic steam reforming over nanoscale CeO_2-based catalysts

N. Laosiripojana [a,*], S. Charojrochkul [b], P. Kim-Lohsoontorn [c], S. Assabumrungrat [d]

[a] The Joint Graduate School of Energy and Environment, CHE Center for Energy Technology and Environment, King Mongkut's University of Technology Thonburi, Thailand
[b] National Metal and Materials Technology Center (MTEC), Pathumthani, Thailand
[c] Department of Chemical Engineering, Faculty of Engineering, Mahidol University, Thailand
[d] Department of Chemical Engineering, Faculty of Engineering, Chulalongkorn University, Thailand

ARTICLE INFO

Article history:
Received 4 June 2010
Revised 8 August 2010
Accepted 14 August 2010
Available online 29 September 2010

Keywords:
CeO_2
Steam reforming
H_2S
Hydrogen

ABSTRACT

The activity of nanoscale CeO_2 and doped CeO_2 (with Gd, Y, Nb, La, and Sm) toward the steam reforming of CH_4 in the presence of H_2S was investigated for later application as an in-stack reforming catalyst in a solid oxide fuel cell. Although H_2S is commonly known as a poisonous gas for metallic-based catalysts, it was found that the presence of appropriate H_2S content increases the reforming activity of these CeO_2-based catalysts. According to postreaction catalyst characterizations by X-ray diffraction, X-ray photoelectron spectroscopy, temperature-programmed reduction, temperature-programmed desorption, $H_2/H_2O + H_2S$ titration, and $^{18}O/^{16}O$ isotope exchange, it was revealed that this behavior is related to the formation of various Ce–O–S phases ($Ce(SO_4)_2$, $Ce_2(SO_4)_3$, and Ce_2O_2S) during the reaction. Our studies indicated that the formation of $Ce(SO_4)_2$ promotes the oxygen storage capacity, the lattice oxygen mobility, and eventually the reforming activity, whereas the formation of Ce_2O_2S oppositely reduces both properties and lowers the reforming rate.

1. Introduction

Hydrogen is widely regarded as a promising energy carrier for fuel cells to generate energy with great improvements in air quality, human health, and climate [1]. It can be produced readily from the reforming of hydrocarbons with oxygen-containing co-reactants [2–5]. Metallic catalysts such as Ni, Rh, and Pd are known to be active for these reactions, but catalyst deactivation due to carbon formation and sulfur poisoning is a major concern when heavy hydrocarbons and/or sulfur-containing feeds such as natural gas, biogas, and liquefied petroleum gas are used [6,7]. Typically, prereforming and/or desulfurization units are needed to reform these feedstocks; however, both installations reduce the flexibility and the potential for applying hydrogen/fuel cell technologies. Research on developing catalysts with high resistance to carbon formation and sulfur interaction is therefore continuing.

Cerium oxide (CeO_2) is extensively used as a catalyst and support for a variety of reactions involving oxidation of hydrocarbons [4,8,9]. This material contains a high concentration of highly mobile oxygen vacancies, which act as local sources or sinks for oxygen involved in reactions taking place on its surface; this behavior renders CeO_2-based materials of interest for a wide range of catalytic applications [10–13]. One of the great potential applications of CeO_2-based material is in solid oxide fuel cells (SOFC) as cell materials and in-stack reforming catalysts (IIR-SOFC) [14–19]. Furthermore, doping CeO_2 with Gd, Nb, La, and Sm has also been reported to improve the redox properties of CeO_2, and these doped forms are now widely used as catalysts in a wide variety of reactions involving oxidation or partial oxidation of hydrocarbons (e.g., automotive catalysis). Previously, we successfully synthesized nano-scale CeO_2 with high specific surface area and thermal stability by a cationic surfactant-assisted method [20]. We then studied H_2O and CO_2 reforming of CH_4, C_2H_4, C_2H_6, C_3H_8, C_4H_{10}, CH_3OH, and C_2H_5OH over this ultrafine CeO_2 and found that this material efficiently converts these hydrocarbons to H_2-rich gas with high resistance toward carbon formation under given conditions [20,21]. We proposed that the turnover rates are strongly influenced by the amount of lattice oxygen (O_O^x) in CeO_2, whereas the kinetic dependencies of hydrocarbon conversions and the activation energies were unaffected by the material's specific surface area, the doping element, the degree of oxygen storage capacity (OSC), and the reactions (i.e., H_2O reforming and CO_2 reforming). Furthermore, identical turnover rates for H_2O and CO_2 reforming (at similar C_nH_m partial pressure) with linear dependence on C_nH_m partial pressure and independence of CO_2 and H_2O partial pressures were observed. These results provide strong evidence that the sole kinetically relevant elementary step is the reaction of intermediate surface hydrocarbon species with O_O^x

* Corresponding author. Fax: +66 662 872 6736.
E-mail address: navadol_l@jgsee.kmutt.ac.th (N. Laosiripojana).

0021-9517/$ - see front matter © 2010 Elsevier Inc. All rights reserved.
doi:10.1016/j.jcat.2010.08.015

and that oxygen is replenished by a rapid surface reaction of reduced-state CeO_2 with oxygen sources (i.e., CO_2 or H_2O) in the system [21].

Recently, the regenerative H_2S adsorption capability of CeO_2 at high temperature was reported [22]. In the present work, the activity of CeO_2 and doped CeO_2 (with several rare earths, Gd, Y, Nb, La, and Sm), synthesized by a cationic surfactant-assisted method, toward the steam reforming of CH_4 in the presence of H_2S was investigated under several operating conditions (i.e., various inlet H_2S contents, inlet steam/carbon (S/C) molar ratios, and operating temperatures). Several characterizations, including X-ray diffraction (XRD), X-ray photoelectron spectroscopy (XPS), temperature-programmed reduction (TPR), temperature-programmed desorption (TPD) under reducing conditions, $H_2/H_2O + H_2S$ titration, and $^{18}O/^{16}O$ isotope exchange methods were also performed over the fresh and spent catalysts from the reactions in order to observe the changes in catalyst phase formation and the redox properties associated with the OSC and the mobility of lattice oxygen. Based on the experimental results and the above analyses, the mechanism of methane steam reforming in the presence of H_2S over nano-scale CeO_2-based catalysts was established. In addition, a practical application with respect to the study using this ultrafine CeO_2 as a primary reforming catalyst to reform natural gas, biogas, and liquefied petroleum gas (LPG) without prior desulfurization was proposed.

2. Experimental

2.1. Catalyst preparations

Nano-scale CeO_2-based materials were synthesized by a cationic surfactant-assisted method. We previously reported that the preparation of ceria-based materials by this method can provide materials with ultrafine particle size, high surface area, and good stability after thermal treatment [20,21]. The achievement of high-surface-area material with good thermal stability by this preparation technique is related to the interaction of hydrous oxide with cationic surfactants under basic conditions and the incorporation of surfactants during preparation, which reduces the interfacial energy and eventually decreases the surface tension of water contained in the pores. It has been reported that this incorporation reduces the shrinkage and collapse of the catalyst during heating, which consequently helps the catalyst maintain high surface area after calcination [23]. In the present work, the undoped CeO_2 was prepared by mixing 0.1 M of cerium nitrate ($Ce(NO_3)_3{\cdot}H_2O$ from Aldrich) solution with 0.1 M of cetyltrimethylammonium bromide (from Aldrich) and keeping the [Ce]/[cetyltrimethylammonium bromide] molar ratio constant at 0.8. This solution was stirred by magnetic stirring (100 rpm) for 3 h and then aqueous ammonia was slowly added until the pH was 11.5. The mixture was continually stirred, sealed, and placed in a thermostatic bath maintained at 263 K. The precipitate was then filtered and washed with deionized water and acetone to remove the free surfactant. It was dried overnight in ambient air at 110 °C and then calcined in flowing dry air by increasing the temperature to 900 °C at a rate of 0.167 °C s^{-1} and holding at 900 °C for 6 h. After calcination, fluorite-structured CeO_2 with good homogeneity was obtained. According to the SEM image (Fig. 1), ultrafine particles of CeO_2 can be achieved from this method (compared to the microscale CeO_2 obtained from the conventional precipitation method). Doped CeO_2 with Gd, Y, Nb, La, and Sm was prepared by mixing $Ce(NO_3)_3$ with $RE(NO_3)_x$ (Re = Gd, Nb, La, Y, and Sm) to achieve a RE ratio in the material of 0.1; $RE_{0.1}$–CeO_2 (in the presence of 0.1 M cetyltrimethylammonium bromide solution). After treatments, the specific surface areas of all doped and undoped CeO_2 were determined by BET measurement (Table 1), and as expected, the surface area for all ceria decreased at high calcination temperatures.

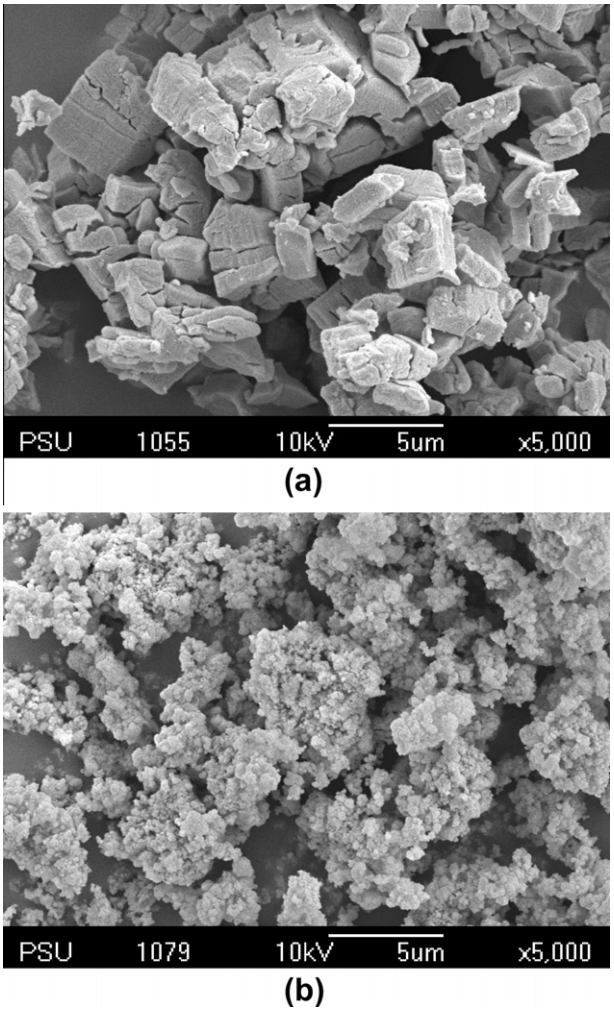

Fig. 1. SEM micrograph of (a) CeO_2 prepared by precipitation method and (b) CeO_2 prepared by cationic surfactant-assisted method (after calcination at 900 °C).

Table 1
Specific surface area of ceria-based materials at several calcination temperatures.

Catalysts	Surface area ($m^2\ g^{-1}$) after calcination at		
	700 °C	800 °C	900 °C
CeO_2	52	35	18
La-doped CeO_2	68	51	26
Gd-doped CeO_2	61	47	23
Sm-doped CeO_2	62	45	23
Nb-doped CeO_2	40	23	11
Y-doped CeO_2	59	41	20

It is noted that, for comparison, Ni/Al_2O_3 and Rh/Al_2O_3 (5 wt.% Ni and Rh) were also prepared and tested toward the steam reforming reaction. In detail, these catalysts were prepared by the wet impregnation of α-Al_2O_3 with aqueous solutions of $Ni(NO_3)_2$ and $Rh(NO_3)_2$ (from Aldrich). According to the fresh catalyst (after reduction) characterizations by X-ray fluorescence (XRF) analysis, temperature-programmed reduction (TPR) with 5% H_2 in helium, and temperature-programmed desorption (TPD) studies, the Ni and Rh weight content was 4.9% and 5.1%, the metal reducibility was 92.1% and 94.8%, and the metal reducibility percentage was 4.87% and 5.04%, respectively.

2.2. Catalytic steam reforming and relevant reactions

To undertake the reaction testing, an experimental reactor system was constructed. The feed gases, including the components of interest, i.e. CH_4, natural gas, biogas, LPG, and H_2S, were controlled and introduced to the system by the mass flow controllers, while deionized H_2O was fed by a syringe pump passing through an evaporator. For methane steam reforming testing, the inlet concentration of CH_4 was 20%, whereas the steam concentration was varied to achieve H_2O/CH_4 ratios between 0.5 and 3.0 and the inlet H_2S concentration was between 10 and 1000 ppm to capture a range of H_2S content in various fuels. As for the steam reforming of sulfur-containing fuels (i.e., natural gas, biogas, LPG) testing, the inlet concentration of total hydrocarbons in these fuels was kept constant at 20%, whereas various steam concentrations were added to achieve S/C ratios between 0.5 and 3.0. It is noted that the reforming tests with and without predesulfurization of these hydrocarbons were compared. Regarding the desulfurization unit, ZnO was applied to adsorb H_2S from the feed (the outlet gases were rechecked by gas chromatography with a flame photometric detector (FPD) to ensure that all H_2S were removed before purging to the reforming testing unit).

The inlet gas mixtures were introduced to the reaction section, in which a 10-mm-diameter quartz reactor was mounted vertically inside a tubular furnace. The catalysts (500 mg) were diluted with SiC (to obtain a total weight of 3.0 g) in order to avoid temperature gradients and loaded into the quartz reactor, which was packed with quartz wool to prevent the catalyst from moving. In the system, a type-K thermocouple was placed in the annular space between the reactor and furnace. This thermocouple was mounted in close contact with the catalyst bed to minimize the temperature difference. It is noted that another type-K thermocouple, covered by a closed-end quartz tube, was inserted into the middle of the quartz reactor in order to recheck the possible temperature deviation due to the heat transfer limitation. The record showed that the maximum temperature fluctuation during the reaction was always ±0.75 °C or less from the temperature specified for the reaction. After the reactions, the exit gas mixture was transferred via trace-heated lines (100 °C) to the analysis section, which consisted of a Porapak Q column Shimadzu 14B gas chromatograph (GC) and a quadrupole mass spectrometer (MS). The GC was applied in the steady state studies, whereas the MS was used for the transient experiments. In the present work, the outlet of the GC column was directly connected to a thermal conductivity detector (TCD), frame ionization detector, and FPD. In order to satisfactorily separate all elements, the temperature setting inside the GC column was programmed to vary with time. In the first 3 min, the column temperature was constant at 60 °C; it was then increased steadily at a rate of 15 °C min^{-1} to 120 °C and last decreased to 60 °C.

In this study, the catalyst activity was identified in terms of the turnover frequencies, H_2 yields, and other outlet gas selectivities. The turnover frequencies can be calculated from the equation [18]

$$\text{turnover frequencies} = \frac{rN_A A_{N_2}}{m_c S} \tag{1}$$

where r is the moles of CH_4 (or hydrocarbons) changing per unit time (mol_{CH_4} min^{-1}), N_A is Avogadro's number, A_{N_2} is the area occupied by an adsorbed nitrogen molecule (16.2×10^{-20} m^2); it is assumed that all surface sites accessible by nitrogen adsorption. m_c is the weight of catalyst used, and S is the specific surface area of the catalyst (m^2 g^{-1}). The yield of H_2 production (Y_{H_2}) was defined as the molar fraction of H_2 produced out of the total hydrogen-based compounds in the products. Other by-product selectivities (i.e., S_{CO}, S_{CO_2}, S_{CH_4}, $S_{C_2H_6}$, and $S_{C_2H_4}$) were defined as the mole ratios of the specified component in the outlet gas to the total carbon-based compounds in the product, accounting for stoichiometry. The following equations present the calculations of these selectivities:

$$S_{CO} = 100 \times \left(\frac{(\%CO)}{(\%CO) + (\%CO_2) + (\%CH_4) + 2(\%C_2H_6) + 2(\%C_2H_4)}\right) \tag{2}$$

$$S_{CO_2} = 100 \times \left(\frac{(\%CO_2)}{(\%CO) + (\%CO_2) + (\%CH_4) + 2(\%C_2H_6) + 2(\%C_2H_4)}\right) \tag{3}$$

$$S_{CH_4} = 100 \times \left(\frac{(\%CH_4)}{(\%CO) + (\%CO_2) + (\%CH_4) + 2(\%C_2H_6) + 2(\%C_2H_4)}\right) \tag{4}$$

$$S_{C_2H_4} = 100 \times \left(\frac{2(\%C_2H_4)}{(\%CO) + (\%CO_2) + (\%CH_4) + 2(\%C_2H_6) + 2(\%C_2H_4)}\right) \tag{5}$$

$$S_{C_2H_6} = 100 \times \left(\frac{2(\%C_2H_6)}{(\%CO) + (\%CO_2) + (\%CH_4) + 2(\%C_2H_6) + 2(\%C_2H_4)}\right) \tag{6}$$

It is noted that, for the studies on methane and biogas steam reforming, the terms for C_2H_6 and C_2H_4 are eliminated.

2.3. Measurement of carbon formation

After reaction, temperature-programmed oxidation (TPO) was used to investigate the amount of carbon formed on the spent catalyst surface by introducing 10% O_2 in helium, after the system was purged with helium. The operating temperature increased from room temperature to 1000 °C at a rate of 10 °C min^{-1}. The amount of carbon formation on the surface of catalysts was determined by measuring the CO and CO_2 yields from the TPO results (using Microcal Origin Software). The calibrations of CO and CO_2 were performed by injecting a known amount of these calibration gases from the sampling loop. In addition to the TPO method, the amount of carbon deposition was confirmed by the carbon balance calculation, in which the amount of carbon deposition theoretically equals the difference between the inlet hydrocarbon fuel and the outlet carbon components (e.g., CO, CO_2, CH_4, and C_{2+}).

2.4. The study of CeO_2 as prereforming catalyst

In the present work, a practical application using CeO_2 as a primary reforming catalyst to reform natural gas, biogas, and LPG (without prior desulfurization) was investigated. In detail, CeO_2 was applied to adsorb H_2S from the feed and primarily reform heavy hydrocarbons (C_{2+}) to light hydrocarbon (i.e., CH_4). The product from this section was continuously passed though a secondary reforming bed, where Ni/Al_2O_3 was packed, to complete the conversion and maximize H_2 yield. The design of this system consists of two tubular-containing CeO_2 columns and one Ni/Al_2O_3 column (with diameters of 25 mm and lengths of 50 cm). In each column, 25 g of either CeO_2 or Ni/Al_2O_3 (mixed with SiC) was packed, and these three columns were placed in the same burner, in which the temperature was controlled isothermally at SOFC temperature (900 °C) for later application as IIR-SOFC. Details of system operation are presented in Section 3.5.

3. Results and discussion

3.1. Preliminary experiments

Preliminary experiments were carried out to find a suitable condition under which internal and external mass transfer effects are

not predominant. Considering the effect of external mass transfer, the total gas flow rate was varied between 10 and 200 $cm^3\ min^{-1}$ for a constant residence time of $5 \times 10^{-4}\ g_{cat}\ min\ cm^{-3}$. It was found that the turnover frequencies are independent of the gas velocity when the gas flow rate is higher than 60 $cm^3\ min^{-1}$, indicating the absence of external mass transfer effects at this high velocity (Fig. 2). Furthermore, the reaction on different average sizes of catalyst was studied in order to ensure that the experiments were carried out within the region of intrinsic kinetics. It was observed that the catalysts with particle size less than 200 μm showed no intraparticle diffusion limitation under the range of conditions studied. Therefore, in the following studies, the total flow rate was kept constant at 100 $cm^3\ min^{-1}$, whereas the catalyst diameters were kept within the above-mentioned range in all experiments.

3.2. Activity of CeO_2 toward steam reforming of CH_4 in the presence of H_2S

First, the steam reforming of CH_4 over nano-scale CeO_2 in the presence of various H_2S contents was investigated. In our studies, H_2S contents of 10, 100, 500, and 1000 ppm (capturing a range of H_2S content in various fuels) were added during the reaction at 900 °C with an H_2O/CH_4 ratio of 3.0. As shown in Fig. 3, we found that the presence of H_2S under appropriate conditions increases the steam reforming rate. Without H_2S, the steady state turnover frequencies were 0.054 s^{-1}. When 10 ppm H_2S was added, the turnover frequencies increased steadily with time and reached a higher steady state value at 0.074 s^{-1}. When more H_2S was added in the feed (100 and 500 ppm), the turnover frequencies increased more rapidly to 0.098 and 0.095 s^{-1}. Nevertheless, when as much as 1000 ppm H_2S was introduced, although the turnover frequencies initially increased to 0.115 s^{-1}, they later gradually dropped to 0.071 s^{-1}. After exposure to H_2S for 3 h, the experiment was continued by removing H_2S from the feed. As also seen in this figure, the turnover frequencies (after 10 ppm H_2S was removed) remain constant, whereas after the experiments with 100 and 500 ppm H_2S the turnover frequencies were slightly reduced to 0.085 and 0.086 s^{-1}, respectively. After 1000 ppm H_2S was removed, the turnover frequencies increased considerably before decreasing to 0.088 s^{-1}. It is noted according to the error analysis that the

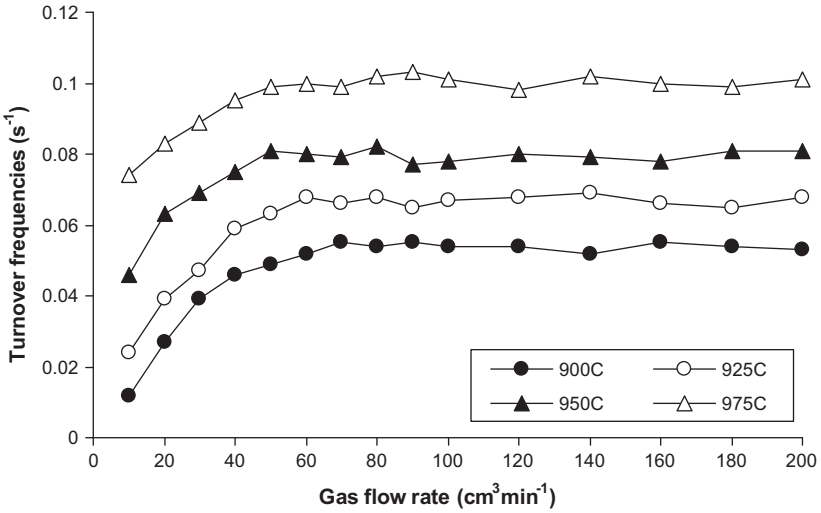

Fig. 2. Effect of the total gas flow rate on the turnover frequencies from the steam reforming at 900–975 °C with constant residence time 5×10^{-4} g min cm^{-3}.

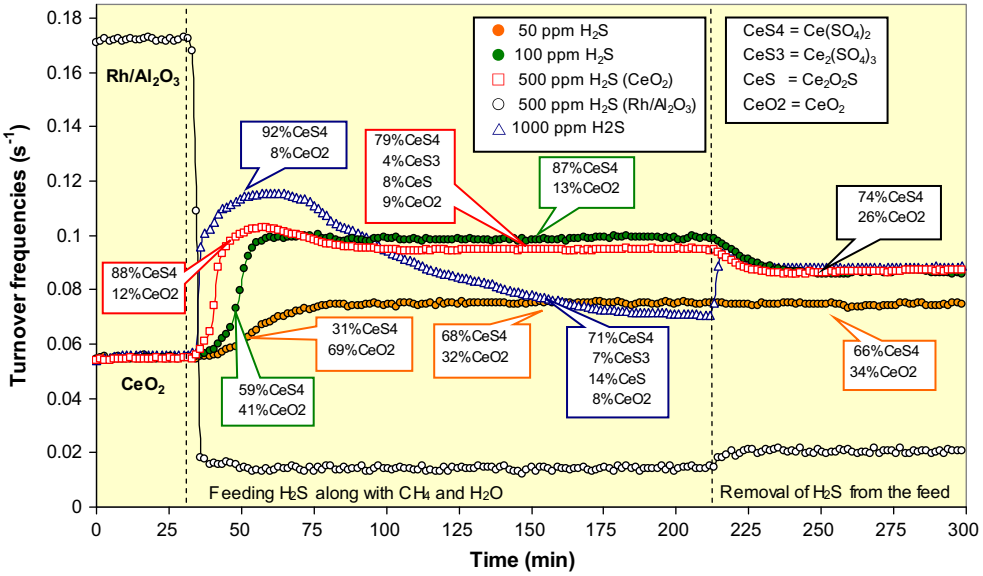

Fig. 3. Effect of H_2S on the turnover frequencies from methane steam reforming and Ce–O–S phase compositions at various H_2S concentrations.

deviations of these turnover frequencies are in the range of ±4.5%. Furthermore, the turnover frequencies observed in the present work are in good agreement with the values previously reported in the literature [18,20].

For comparison, the effect of H_2S on the steam reforming activity of highly active Rh/Al_2O_3 was also studied by adding 500 ppm H_2S along with CH_4 and H_2O. It was found that, in the presence of H_2S, the turnover frequencies from the steam reforming over Rh/Al_2O_3 dramatically dropped from 0.172 to 0.013 s^{-1} in a short time and could not be recovered even when H_2S was removed from the system (Fig. 3). It is noted that the XRD study on the spent Rh/Al_2O_3 catalyst indicated the formation of rhodium sulfide, which is rarely regenerated.

3.3. Effects of temperature and inlet H_2O/CH_4 ratio

As the next step, the effects of operating temperature and inlet H_2O/CH_4 molar ratio on the steam reforming of CH_4 over CeO_2 in the presence of H_2S were determined by varying the temperature (from 900 °C to 925, 950, and 975 °C) and inlet H_2O/CH_4 molar ratio (from 3.0 to 2.0, 1.5, and 1.0). It was found that the influence of H_2S on the turnover frequencies over CeO_2 strongly depends on the operating temperature and inlet H_2O/CH_4 ratio (Fig. 4). When 100 ppm H_2S was added at 900 °C, the turnover frequencies increased by 81% (from 0.054 to 0.098 s^{-1}); this difference increased to 83% (from 0.063 to 0.117 s^{-1}), 86% (from 0.075 to 0.139 s^{-1}), and 88% (from 0.089 to 0.168 s^{-1}) when the temperature increased to 925, 950, and 975 °C, respectively. In contrast, at 900 °C, when the inlet H_2O/CH_4 ratio was reduced to 2.0, 1.5, and 1.0, the positive deviation of the turnover frequencies with H_2S was reduced to +53%, +25%, and +7.9%; and when an H_2O/CH_4 ratio below 1.0 was applied, H_2S then reduced the turnover frequencies (from 0.054 s^{-1} to 0.041, 0.038, and 0.033 s^{-1} at inlet H_2O/CH_4 ratios of 0.75, 0.5, and 0.25). It is suggested from the XRD studies on spent CeO_2 after several reaction periods and conditions that this contradictory effect of H_2S is related to the formation of various Ce–O–S phases: $Ce(SO_4)_2$, $Ce_2(SO_4)_3$, and Ce_2O_2S, during the reaction (as illustrated in Fig. 5). The relevant reactions between CeO_2 and H_2S, which result in these phases, may be.

$$2CeO_2 + 8H_2O + 3H_2S \leftrightarrow Ce_2(SO_4)_3 + 11H_2 \quad (7)$$

$$Ce_2(SO_4)_3 + 4H_2O + H_2S \leftrightarrow 2Ce(SO_4)_2 + 5H_2 \quad (8)$$

$$2CeO_2 + H_2 + H_2S \leftrightarrow Ce_2O_2S + 2H_2O \quad (9)$$

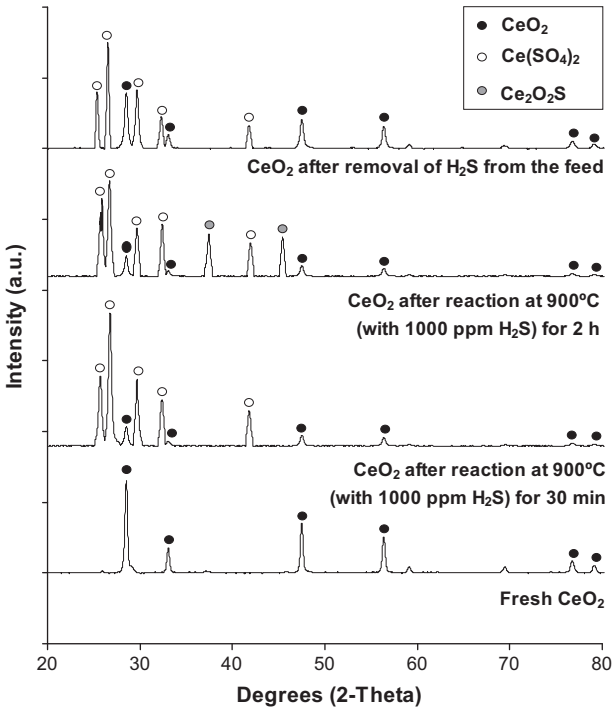

Fig. 5. XRD patterns of CeO_2 at various reaction times.

When 10 and 100 ppm H_2S was introduced during the reaction (with an H_2O/CH_4 ratio of 3.0 at 900 °C), $Ce(SO_4)_2$ was formed (via Eqs. (7) and (8)) and its proportion increased with increasing operating time (from 31% after 20 min to 68% after 2 h for 10 ppm H_2S; and from 59% after 20 min to 87% after 2 h for 100 ppm H_2S). In the experiments with 500 and 1000 ppm H_2S, as well as $Ce(SO_4)_2$ formation (79% and 71% for 500 and 1000 ppm H_2S), $Ce_2(SO_4)_3$ (4% and 7% for 500 and 1000 ppm H_2S) and Ce_2O_2S (8% and 14% for 500 and 1000 ppm H_2S) were also observed. At higher operating temperatures, the portion of $Ce(SO_4)_2$ phase increased considerably. On the other hand, when inlet H_2O/CH_4 ratios less than 1.0 were applied, Ce_2O_2S (occurs via Eq. (9)) became the dominant Ce–O–S phase. It has been suggested that with decreasing oxygen fugacity, the sulfate form of ceria decomposes to CeO_2 and then to

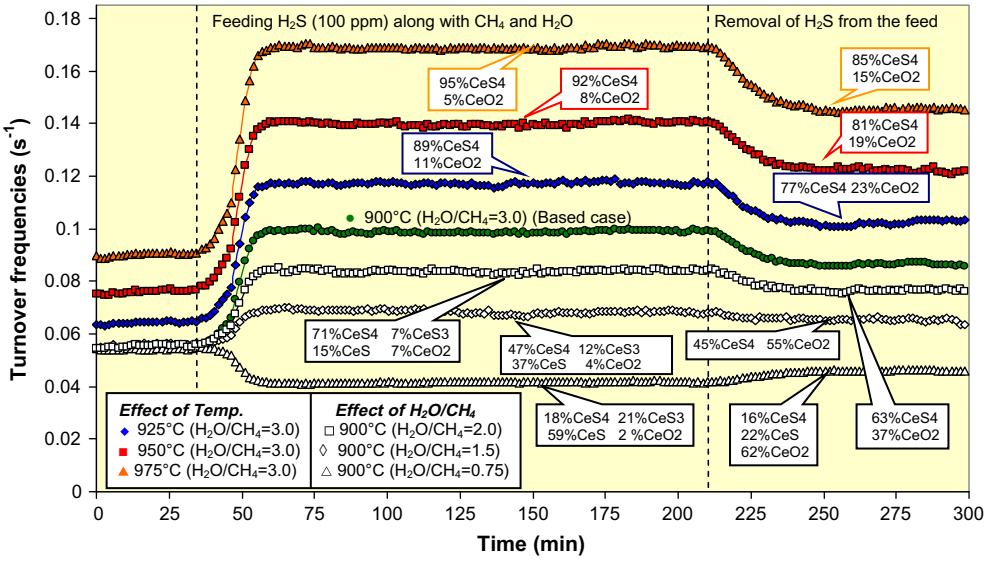

Fig. 4. Effect of H_2S on the turnover frequencies from methane steam reforming and Ce–O–S phase compositions at various temperatures and H_2O/CH_4 ratios.

Ce_2O_2S [24]. After H_2S removal, XRD patterns revealed that the Ce_2O_2S phase disappeared (due to the reversal of Eq. (9)), while the portion of $Ce(SO_4)_2$ phase slightly decreased but that of the CeO_2 phase increased.

3.4. Determination of the OSC and lattice oxygen mobility

Based on the results from Sections 3.1 and 3.2, we suggest that the formation of $Ce(SO_4)_2$ during the reaction leads to a high reforming activity, whereas the presence of Ce_2O_2S reduces the activity. To test this idea, the redox properties associated with the OSC and the mobility of lattice oxygen for $Ce(SO_4)_2$ were examined and compared to those for CeO_2 by applying TPR, TPD under reducing condition, $H_2/H_2O + H_2S$ titration, and $^{18}O/^{16}O$ isotope exchange methods. Furthermore, the ratio of Ce^{3+}/Ce^{4+} under reducing and oxidizing conditions was characterized by XPS. In detail, the TPR experiment was carried out in a 10-mm-diameter quartz reactor, which was mounted vertically inside tubular furnace. A type-K thermocouple was placed into the annular space between the reactor and furnace, while another thermocouple, covering by a closed-end quartz tube, was inserted into the middle of the quartz reactor in order to recheck the possible temperature gradient. The sample (100 mg) was heated from 25 to 1000 °C under 5% H_2 in nitrogen with a flow rate of 50 $cm^3\ min^{-1}$, and the amount of H_2 consumed during the TPR process at different temperatures was monitored online by the TCD and quantified by calibrating the peak areas against the TPR of a known amount of CuO. The TPD over $Ce(SO_4)_2$ under the reducing-condition experiment was performed in the same scale of reactor with the same weight of sample as the TPR study (under 5%H_2 in nitrogen), but the effluent gases from the TPD experiment were monitored by the MS. It is noted that the MS signals were calibrated with a known amount of outlet gases (e.g., H_2S) to determine the absolute coverages corresponding to these TPD signals. As for $H_2/H_2O + H_2S$ titration, this experiment was conducted over $Ce(SO_4)_2$ to confirm the consecutive cycles of $Ce(SO_4)_2 \leftrightarrow CeO_2 \leftrightarrow Ce_2O_2S$. Similarly to the TPR and TPD experiments, the sample (100 mg of $Ce(SO_4)_2$) was placed in the middle of a quartz reactor packed with two layers of quartz wool to prevent the sample from moving. After the system was purged with helium for 1 h, known amounts of H_2 and $H_2O + H_2S$ were sequentially pulsed to the reactor for five consecutive cycles and the effluent gases were monitored with the MS. Last, an $^{18}O/^{16}O$ isotope exchange experiment was carried out to investigate the lattice oxygen mobility of the samples (CeO_2 and $Ce(SO_4)_2$). The sample (200 mg) was placed in the quartz reactor and thermally treated under a flow of high-purity helium (99.995%) at the desired temperatures for 1 h. Then $^{18}O_2$ (in helium) was multiply pulsed into the system and the outlet gases were monitored by the MS.

We found in the studies that the TPR of $Ce(SO_4)_2$ indicated a sharp reduction band at 470 °C and a broader band at 810 °C, whereas for CeO_2 smaller peaks were detected at slightly higher temperatures (600 and 850 °C). The TPD under reducing conditions showed an amount of H_2S desorption approximately corresponding to half of the initial coverage of sulfate relevant to the formation of Ce_2O_2S. After TPD, all sulfates were reduced to Ce_2O_2S. The $H_2/H_2O + H_2S$ titration was conducted to ensure that Ce_2O_2S can be reoxidized to sulfate forms. In five consecutive cycles, the amounts of H_2 uptake were nearly identical (Fig. 6), suggesting that the redox behavior of $Ce(SO_4)_2$ and CeO_2 is reversible. The amounts of H_2 uptake and H_2S produced were applied to indicate the amount and percentage of reducible oxygen in the catalysts. From the calculation, the amount of reducible oxygen for $Ce(SO_4)_2$ was estimated to be 1.27 mmol g^{-1} (17.3% of total oxygen in catalyst) compared to 0.71 mmol g^{-1} (10.1% of total oxygen in catalyst) for CeO_2; this clearly indicates the higher OSC of $Ce(SO_4)_2$. Furthermore, regarding the $^{18}O/^{16}O$ isotope exchange study, it is known that the exchange of $^{18}O/^{16}O$ isotopes over CeO_2 surface theoretically consists of (i) homoexchange in the gas phase ($^{18}O_2$ (g) + $^{16}O_2$ (g) → $^{18}O^{16}O$ (g)) and (ii) heteroexchange with the participation of oxygen atoms from CeO_2 ($^{18}O_2$ (g) + $^{16}O_2$ (S) → $^{18}O^{16}O$ (g) + ^{18}O (S) and $^{18}O^{16}O$ (g) + $^{16}O_2$ (S) → $^{16}O_2$ (g) + ^{18}O (S)). According to our results at 600 °C, the production of $^{16}O_2$ and $^{18}O^{16}O$ for $Ce(SO_4)_2$ is 24 and 17%, whereas the production of $^{16}O_2$ and $^{18}O^{16}O$ for CeO_2 is 12 and 2%. Therefore, the homoexchange in the gas phase is negligible under these operating conditions, since $^{18}O^{16}O$ concentration from both materials should be identical if the exchange in the gas phase is dominant for the overall reaction [25]. Fig. 7 shows the Arrhenius plots from $^{18}O/^{16}O$ isotope exchange studies over $Ce(SO_4)_2$ compared to CeO_2. It was found that the conversion of $^{18}O_2$ increases with increasing temperature to form $^{16}O_2$ and $^{18}O^{16}O$ for both materials and the production of $^{16}O_2$ and $^{18}O^{16}O$ from $Ce(SO_4)_2$ is greater than that from CeO_2, indicating its higher oxygen mobility. Furthermore, the observed activation energy from $^{18}O/^{16}O$ isotope exchange over $Ce(SO_4)_2$ is 85 kJ mol^{-1}, whereas that over CeO_2 was 110 kJ mol^{-1}.

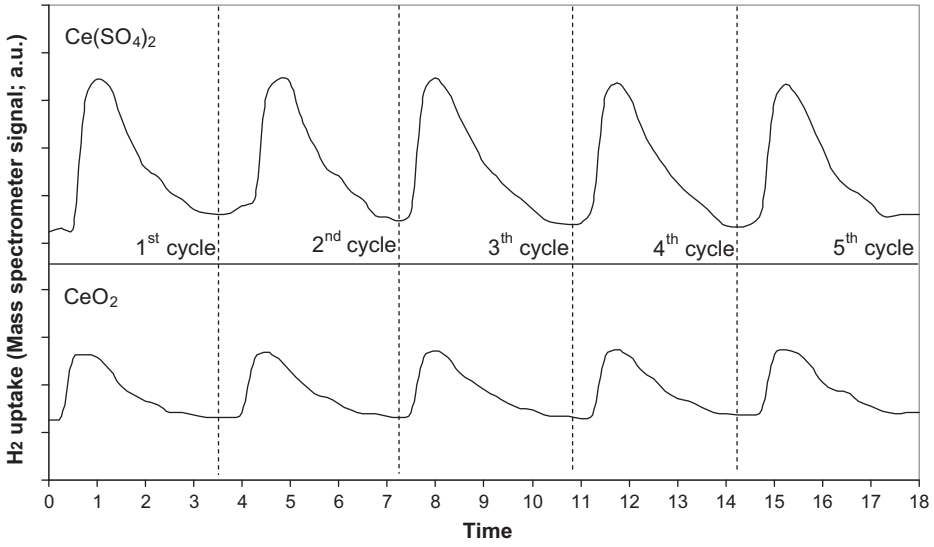

Fig. 6. H_2 uptake from $H_2/H_2O + H_2S$ titration over $Ce(SO_4)_2$ and CeO_2 for five cycles.

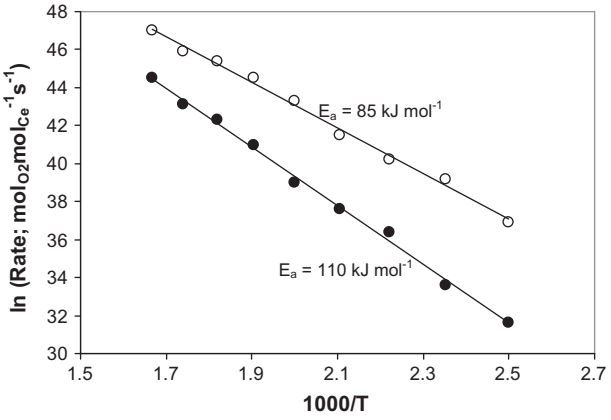

Fig. 7. Arrhenius plots from $^{18}O/^{16}O$ isotope exchange studies over (○) $Ce(SO_4)_2$ and (●) CeO_2.

Last, the XPS studies were also carried out to quantify the Ce^{4+} and Ce^{3+} levels of reduced and oxidized states of sulfate-form samples (Ce_2O_2S and $Ce(SO_4)_2$) compared to reduced and oxidized states of CeO_2. The XPS spectra implied that, under reducing conditions, the contents of Ce^{3+} for the sulfate-form sample and CeO_2 were 34.6% and 24.9%, respectively, while under oxidizing conditions, the contents of Ce^{3+} for the sulfate-form sample and CeO_2 were 17.3% and 19.8%, respectively. These results suggest that CeO_2 in sulfate form promotes the reduction of Ce^{4+} to Ce^{3+} under reducing conditions and the oxidation of Ce^{3+} to Ce^{4+} under oxidizing conditions. It is noted that these results should be further confirmed by an *in situ* XPS study, which can determine the Ce^{4+}/Ce^{3+} values during the reaction. Nevertheless, based on all characterization results, the greater redox properties of $Ce(SO_4)_2$ compared to CeO_2, which lead to the higher reforming activity, can be confirmed.

3.5. Long-term stability testing, effect of doped CeO_2 (with Gd, Y, Nb, La, and Sm), and activity toward the steam reforming of several hydrocarbons

Long-term stability testing with consecutive cycles at various scenarios (i.e., $CH_4 + H_2O/CH_4 + H_2O + H_2S/CH_4 + H_2O$ and $CH_4 + H_2O/CH_4 + H_2O + H_2S/O_2$ with different inlet H_2S concentrations) was carried out (Fig. 8). Over 50 h with 10 cycles, good stability and reversibility were observed for all conditions. Furthermore, the effect of doping CeO_2 with Gd, Y, Nb, La, and Sm on the contradictory behavior of H_2S was also studied, since doping with these rare earths is known to affect the OSC of CeO_2 [26,27]. It was first observed that doping with La, Sm, Gd, and Y increased the turnover frequencies of CeO_2 (which relates to their OSC improvement), whereas doping with Nb shows an inhibitory effect due to the strong segregation of Nb from the CeO_2 surface. It was then found that the effect of H_2S on doped and undoped CeO_2 followed the same trend but with different magnitude depending on the OSC of materials. Based on TPR and H_2–O_2 titration testing, the amounts of reducible oxygen over doped CeO_2 with Gd, Y, Nb, La, and Sm were 0.93, 0.82, 0.45, 1.09, and 0.95 mmol g^{-1} compared to 0.71 mmol g^{-1} for undoped CeO_2. These values are closely related to the turnover frequencies of the materials, in that the order of turnover frequencies without and with 100 ppm H_2S is La–CeO_2 (0.083 s^{-1}/0.121 s^{-1}) > Sm–CeO_2 (0.071 s^{-1}/0.113 s^{-1}) > Gd–CeO_2 (0.069 s^{-1}/0.109 s^{-1}) > Y–CeO_2 (0.061 s^{-1}/0.104 s^{-1}) > undoped CeO_2 (0.054 s^{-1}/0.098 s^{-1}) > Nb–CeO_2 (0.041 s^{-1}/0.066 s^{-1}).

With regard to more practical applications, the steam reforming of sulfur-containing hydrocarbons, i.e., natural gas (67%CH_4, 8.6%C_2H_6, 4.5%C_3H_8, 2.5%C_4H_{10}, and 14.5%CO_2 with 50 ppm H_2S sup-

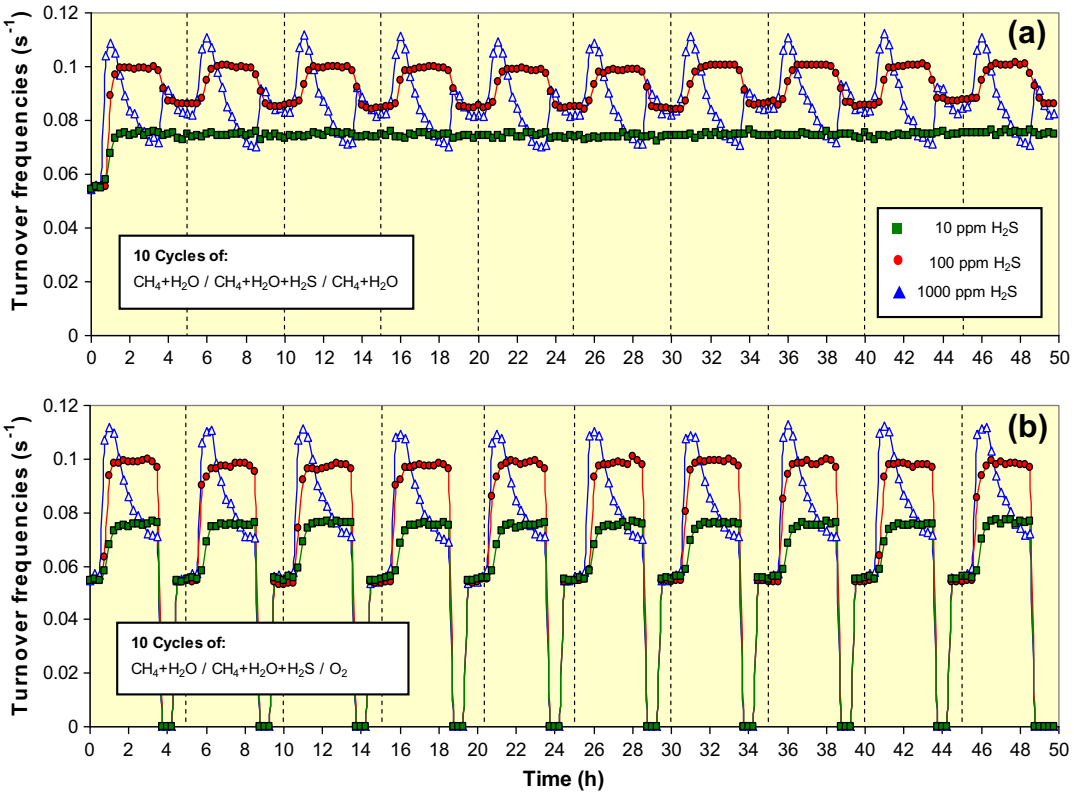

Fig. 8. Prolonged testing with 10 consecutive cycles of $CH_4 + H_2O/CH_4 + H_2O + H_2S/CH_4 + H_2O$ (a) and $CH_4 + H_2O/CH_4 + H_2O + H_2S/O_2$ (b) at three different H_2S concentrations.

Table 2
Turnover frequencies, H_2 yield, and other outlet gas selectivities from the steam reforming of natural gas, LPG, and biogas over CeO_2 at several temperatures and S/C molar ratios (with and without prior desulfurization).

Fuel	Temp. (°C)	S/C ratio	Turnover frequencies (s^{-1})				H_2 yield (%)	By-product selectivity (%)			
			CH_4	C_2H_6	C_3H_8	C_4H_{10}		CO	CO_2	CH_4	C_{2+}
Natural gas	900	3.0	0.070 (0.043)[a]	0.018 (0.017)	0.010 (0.010)	0.006 (0.006)	49 (32)	37 (20)	25 (18)	38 (59)	0 (3)
	925	3.0	0.085 (0.052)	0.019 (0.017)	0.010 (0.010)	0.006 (0.006)	57 (37)	48 (26)	23 (16)	29 (58)	0 (0)
	950	3.0	0.105 (0.059)	0.021 (0.018)	0.010 (0.010)	0.006 (0.006)	69 (41)	57 (32)	21 (15)	22 (53)	0 (0)
	1000	3.0	0.138 (0.078)	100 (0.019)	0.010 (0.010)	0.006 (0.006)	81 (50)	65 (40)	19 (11)	16 (49)	0 (0)
	900	2.0	0.070 (0.043)	0.018 (0.017)	0.010 (0.010)	0.006 (0.006)	48 (30)	39 (23)	23 (15)	38 (59)	0 (3)
	900	1.5	0.056 (0.043)	0.018 (0.017)	0.010 (0.010)	0.006 (0.006)	43 (28)	33 (25)	20 (12)	47 (60)	0 (3)
	900	1.0	0.049 (0.043)	0.017 (0.017)	0.010 (0.010)	0.006 (0.006)	37 (26)	31 (26)	12 (10)	55 (60)	2 (4)
	900	0.5	0.043 (0.038)	0.017 (77)	0.010 (0.010)	0.006 (0.006)	28 (24)	29 (28)	9 (3)	59 (63)	3 (6)
			C_3H_8	C_4H_{10}				CO	CO_2	CH_4	C_{2+}
LPG	900	3.0	0.108 (0.108)	0.108 (0.108)			69 (61)	58 (50)	27 (21)	13 (21)	2 (8)
	925	3.0	0.108 (0.108)	0.108 (0.108)			76 (65)	65 (57)	24 (19)	10 (19)	0.2 (5)
	950	3.0	0.108 (0.108)	0.108 (0.108)			83 (68)	72 (64)	20 (17)	8 (18)	0 (1.4)
	1000	3.0	0.108 (0.108)	0.108 (0.108)			89 (71)	78 (71)	17 (14)	5 (15)	0 (0)
	900	2.0	0.108 (0.108)	0.108 (0.108)			65 (58)	57 (52)	21 (18)	17 (22)	5 (8)
	900	1.5	0.108 (0.108)	0.108 (0.108)			59 (55)	55 (54)	18 (15)	20 (22)	7 (9)
	900	1.0	0.108 (0.108)	0.108 (0.108)			54 (52)	53 (55)	13 (10)	24 (25)	10 (10)
	900	0.5	0.108 (0.108)	0.108 (0.108)			45 (49)	51 (56)	6 (7)	30 (26)	13 (11)
								CO	CO_2	CH_4	
Biogas	900	3.0	0.071 (0.054)				43 (33)	27 (24)	33 (31)	40 (45)	
	925	3.0	0.088 (0.067)				50 (38)	34 (30)	31 (29)	35 (41)	
	950	3.0	0.108 (0.078)				58 (40)	42 (37)	29 (26)	29 (37)	
	1000	3.0	0.147 (0.101)				75 (51)	54 (45)	26 (24)	20 (31)	
	900	2.0	0.062 (0.054)				37 (31)	26 (27)	32 (28)	42 (45)	
	900	1.5	0.056 (0.054)				31 (29)	25 (30)	31 (25)	44 (45)	
	900	1.0	0.047 (0.052)				24 (28)	23 (33)	30 (21)	47 (46)	
	900	0.5	0.041 (0.049)				21 (25)	21 (35)	30 (18)	49 (47)	

[a] Values in blanket are those observed from the steam reforming of feedstocks with prior desulfurization.

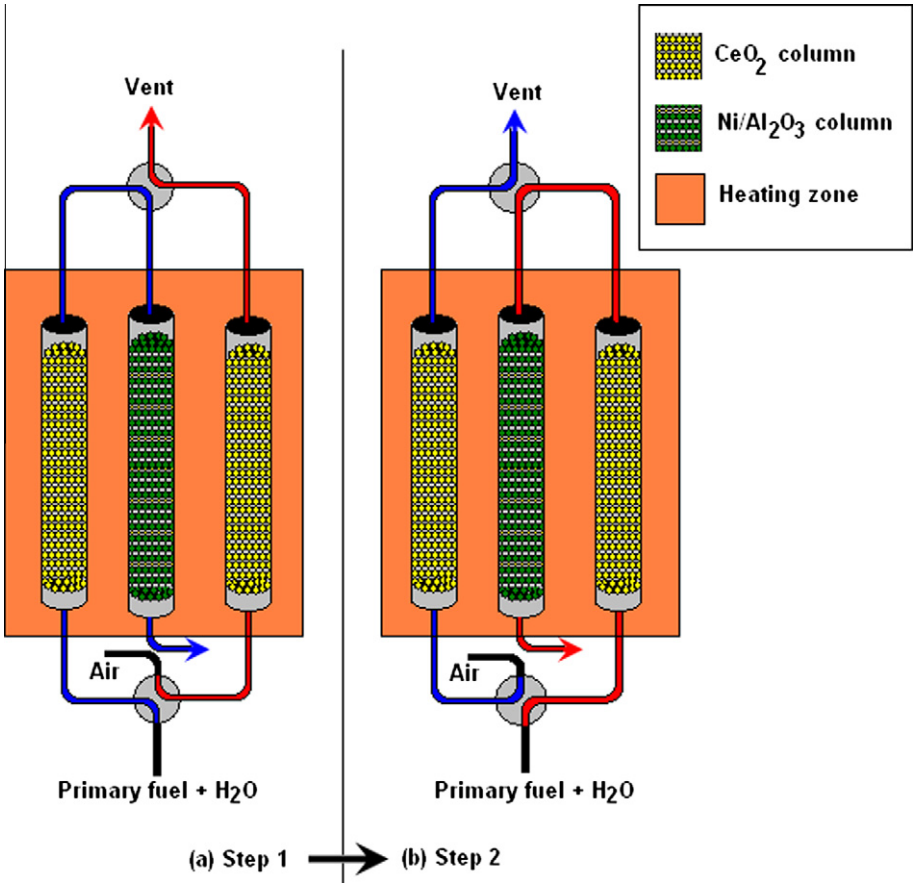

Fig. 9. Design and operation of CeO_2 as prereforming catalyst in the present work.

plied by PPT Plc., Thailand), LPG (60%C_3H_8, 40%C_4H_{10} with 100 ppm H_2S), and biogas (60%CH_4, 40%CO_2 with 1000 ppm H_2S) with and without desulfurization over CeO_2 was examined. Table 2 presents the catalytic activity in terms of turnover frequencies, H_2 yield, and by-product selectivities for various operating conditions. At suitable conditions, i.e., inlet S/C ratio 3.0, higher turnover frequencies could be achieved from the steam reforming of these feedstocks without desulfurization. Furthermore, after reaction for 18 h, the amounts of carbon deposition under each condition were analyzed by TPO and carbon balance calculation. It was found that, with an inlet S/C molar ratio of 3.0, the observed carbon deposition from the steam reforming of natural gas, LPG, and biogas (at 900 °C) was in the range of 0.22–0.26, 0.62–0.65, and 0.04–0.07 mmol g_{cat}^{-1}, respectively. These low amounts of carbon deposition indicate the excellent resistance toward carbon deposition of CeO_2.

Nevertheless, as seen from this table, CeO_2 alone as a reforming catalyst gives relatively low reforming activity and some hydrocarbons (mainly CH_4) were detected in the product, indicating incomplete conversion. Thus, we proposed the pairing of CeO_2 with a suitable metallic catalyst to achieve the benefits of self-desulfurization, improved resistance to carbon deposition, and higher reforming activity. For the approach in the present work, CeO_2 was applied as a prereforming catalyst in order to adsorb H_2S from the feed and primarily reform heavy hydrocarbons (C_{2+}) in the feed to CH_4. The product from this section was continuously passed though a secondary reforming bed, where Ni/Al_2O_3 was packed, to complete the conversion and to maximize H_2 yield. Design and operation of this prototype system are shown in Fig. 9. As for the operation, the primary fuels (i.e., natural gas, LPG, and biogas) were mixed with steam and flowed past a switching valve through the first CeO_2 column to remove all H_2S and partially reform all heavy hydrocarbons to CH_4. At the end of this tube, the gas mixture flowed backward past another switching valve to the Ni/Al_2O_3 column to complete the reforming reaction. At proper

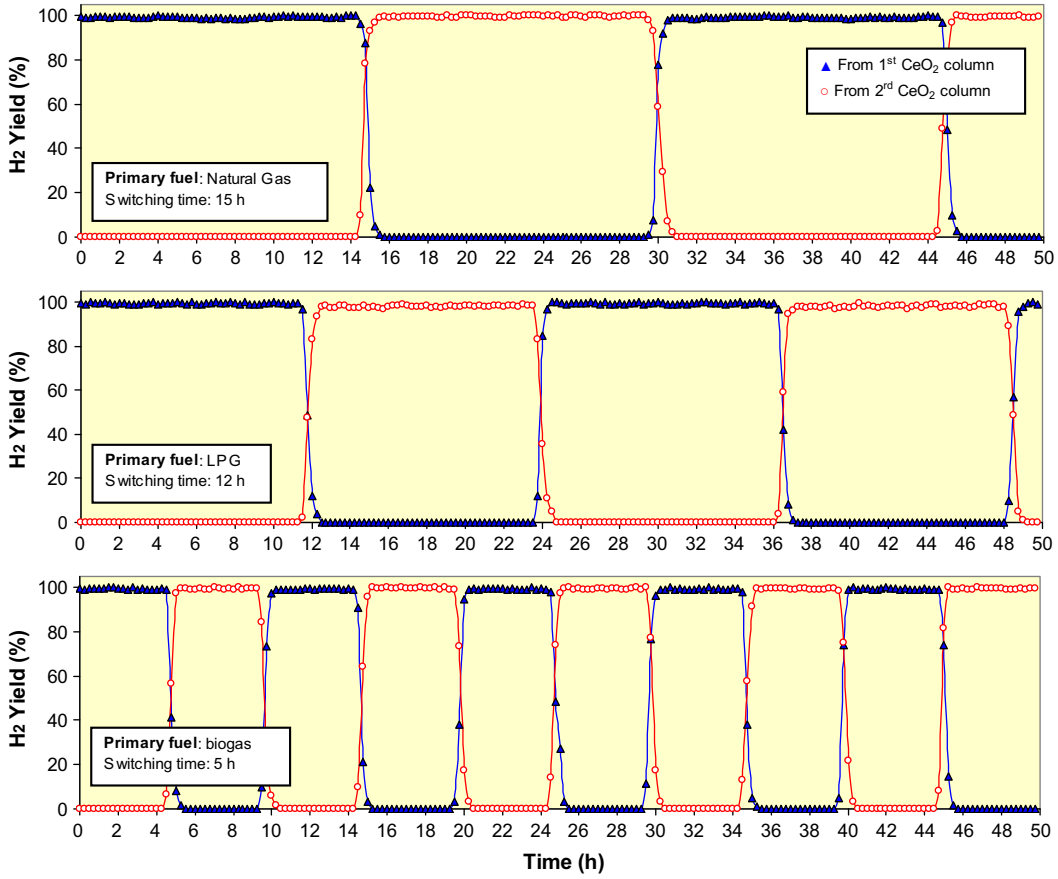

Fig. 10. H_2 yield produced from the use of CeO_2 as prereforming catalyst fed by different primary fuels at 900 °C with appropriate switching times (from first CeO_2 column to second CeO_2 column).

Table 3
Activity in terms of turnover frequencies, H_2 yield, other outlet gas selectivities, and the amount of carbon formation from the steam reforming of natural gas, LPG, and biogas (using CeO_2 as primary reforming catalyst and Ni/Al_2O_3 as secondary reforming catalyst) at 900 °C with S/C molar ratio 3/1.

Fuel	Regeneration time (h)	Turnover frequencies (s^{-1})				H_2 yield (%)	By-product selectivity (%)				Carbon formation (mmol g_{cat}^{-1})
		CH_4	C_2H_6	C_3H_8	C_4H_{10}		CO	CO_2	CH_4	C_2H_4	
Natural gas	15	0.173	0.022	0.011	0.006	99.7	66.3	33.5	0.2	0	0.36[a] (0.33)[b]
LPG	12	–	–	0.108	0.108	99.0	74.6	25.0	0.4	0	0.91 (0.95)
Biogas	5	0.214	–	–	–	99.7	61.3	38.5	0.2	–	0.09 (0.12)

[a] Calculated using CO and CO_2 yields from the TPO study.
[b] Calculated from the balance of carbon-based compounds in the system.

exposure times (5 h for biogas, 12 h for LPG, and 15 h for natural gas, where H_2S start came out in the outlet gas), two switching valves as mentioned above automatically switched the port direction and the primary fuels were flowed through the second CeO_2 column instead. Simultaneously, the air was purged through the first CeO_2 column to remove all sulfur elements in the column and vent out from the system. In our study, the switching process was repeated five times or for 50 h without detection of any activity deactivation, as shown in Fig. 10. The results in Table 3 also indicate that almost 100% H_2 yield could be achieved from all feedstocks; furthermore, low amounts of carbon deposition (less than 1.0 mmol g_{cat}^{-1}) were detected from all reactions after the prolonged testing. We concluded that the novelties of this reforming unit are the flexibility of inlet fuels and the nonrequirements for a desulfurization unit, a separate prereforming unit, and/or the use of expensive noble metal catalysts to reform sulfur-containing heavy hydrocarbon feedstocks. Importantly, this reforming unit would promote the practical application of IIR-SOFC, particularly with the use of a sulfur-tolerant SOFC anode, by eliminating the requirements for costly desulfurization units.

4. Conclusions

The presence of appropriate H_2S content makes it possible to promote the steam reforming rate of nano-scale CeO_2 and doped CeO_2 (with Gd, Y, Nb, La, and Sm). This contradictory effect was related to the formation of various Ce–O–S phases (i.e., $Ce(SO_4)_2$, $Ce_2(SO_4)_3$, and Ce_2O_2S) during the reaction. It was revealed that the formation of $Ce(SO_4)_2$ promotes the OSC, the lattice oxygen mobility, and eventually the reforming activity, whereas the formation of Ce_2O_2S reduces the OSC, the lattice oxygen mobility, and the reforming rate. The capability of these CeO_2 catalysts to adsorb and use poisoning H_2S gas to enhance its catalytic activity offers great benefits in terms of energy and environmental management, and importantly, this behavior would help to promote the hydrogen/fuel cell economy by eliminating the requirements for costly desulfurization units.

Acknowledgments

Financial support from the Thailand Research Fund (TRF) throughout this project is gratefully acknowledged. The authors acknowledge Dr. John T.H. Pearce for the English correction of this manuscript.

References

[1] M.Z. Jacobson, W.G. Colella, D.M. Golden, Science 308 (2005) 901.
[2] J.R. Rostrup-Nielsen, J. Sehested, J.K. Nørskov, Adv. Catal. 47 (2002) 65.
[3] J.R. Rostrup-Nielsen, T.S. Christensen, I. Dybkjaer, Stud. Surf. Sci. Catal. 113 (1998) 81.
[4] G.A. Deluga, J.R. Salge, L.D. Schmidt, X.E. Verykios, Science 303 (2004) 993.
[5] G.W. Huber, J.W. Shabaker, J.A. Dumesic, Science 300 (2003) 2075.
[6] J.R. Rostrup-Nielsen, Stud. Surf. Sci. Catal. 147 (2004) 121.
[7] G. Jones, J.G. Jakobsen, S.S. Shim, J. Kleis, M.P. Andersson, J. Rossmeisl, F. Abild-Pedersen, T. Bligaard, S. Helveg, B. Hinnemann, J.R. Rostrup-Nielsen, I. Chorkendorff, J. Sehested, J.K. Nørskov, J. Catal. 259 (2008) 147.
[8] A. Grirrane, A. Corma, H. García, Science 322 (2008) 1661.
[9] J.A. Rodriguez, S. Ma, P. Liu, J. Hrbek, J. Evans, M. Pérez, Science 318 (2007) 1757.
[10] A. Trovarelli, Catal. Rev. Sci. Eng. 38 (1996) 439.
[11] P. Fornasiero, G. Balducci, R.D. Monte, J. Kaspar, V. Sergo, G. Gubitosa, A. Ferrero, M. Graziani, J. Catal. 164 (1996) 173.
[12] T. Miki, T. Ogawa, M. Haneda, N. Kakuta, A. Ueno, S. Tateishi, S. Matsuura, M. Sato, J. Phys. Chem. 94 (1990) 339.
[13] C.T. Campbell, C.H.F. Peden, Science 309 (2005) 713.
[14] T. Hibino, A. Hashimoto, T. Inoue, J. Tokuno, S. Yoshida, M. Sano, Science 288 (2000) 2031.
[15] Z. Zhan, S.A. Barnett, Science 308 (2005) 844.
[16] R.J. Gorte, J.M. Vohs, S. McIntosh, Solid State Ion. 175 (2004) 1.
[17] O. Costa-Nunes, R.J. Gorte, J.M. Vohs, J. Power Sources 141 (2005) 241.
[18] E. Ramírez-Cabrera, A. Atkinson, D. Chadwick, Appl. Catal. B 47 (2004) 127.
[19] D.J.L. Brett, A. Atkinson, D. Cumming, E. Ramírez-Cabrera, R. Rudkin, N.P. Brandon, Chem. Eng. Sci. 60 (2005) 5649.
[20] N. Laosiripojana, S. Assabumrungrat, Appl. Catal. B 60 (2005) 107.
[21] N. Laosiripojana, S. Assabumrungrat, Appl. Catal. B 82 (2008) 103.
[22] M. Flytzani-Stephanopoulos, M. Sakbodin, Z. Wang, Science 312 (2006) 1508.
[23] D. Terribile, A. Trovarelli, J. Llorca, C. Leitenburg, G. Dolcetti, J. Catal. 178 (1998) 299.
[24] D.A.R. Kay, W.G. Wilson, V. Jalan, J. Alloys Compd. 192 (1993) 11.
[25] Y. Zeng, S. Kaytakoglu, D.P. Harrison, Chem. Eng. Sci. 55 (2000) 4893.
[26] H. He, H.X. Dai, K.W. Wong, C.T. Au, Appl. Catal. A 251 (2003) 61.
[27] L. Cao, C. Ni, Z. Yuan, S. Wang, Catal. Commun. 10 (2009) 1192.